Environmental Science and Pollution Research (2022) 29:80353–80365
https://doi.org/10.1007/s11356-022-20961-0

RESEARCH ARTICLE

Carbon-based zero valent iron catalyst for NO_X removal at low temperatures: performance and kinetic study

Wan Cao[1] · Weijun Zhang[1] · Ziyang Guo[1]

Received: 16 March 2022 / Accepted: 16 May 2022 / Published online: 18 June 2022

Abstract

In order to solve the problem of nitrous oxide (NO_X) removal at low temperatures, the carbon-based zero valent iron (C-ZFe) catalyst was prepared and studied. According to the kinetic study and the obtained kinetic parameters, the De-NO_X reactor was designed to provide information for industrial applications. The box-behnken experimental design (BBD) was used to study the performance of C-ZFe, and the optimized operating parameters were obtained as the temperature was 408.15 K, the catalyst bed height was 140 cm (the space velocity was 459 h^{-1}), the concentration of NO was 550 ppm, under which the NO_X conversion was 72.7%. A kinetic model based on Langmuir–Hinshelwood (L–H) and Mars Van Krevelen mechanism was used to describe the kinetics for the reduction of NO by C-ZFe at low temperatures. Scanning electron microscopy (SEM), energy dispersive spectroscopy (EDS), surface area and pore size distribution measurements, X-ray diffraction (XRD), and X-ray photoelectron spectroscopy (XPS) results supported the validity of the model proposed. The gas–solid catalytic kinetic process of NO removal by C-ZFe was a quasi-first-order kinetic reaction, the apparent activation energy was 41.57 kJ/mol, and the pre-exponential factor was 2980 min^{-1}.

Keywords Low temperature, · Nitrous oxide, · Supported catalysts, · Transition metal, · Activated carbon

Introduction

Nitrous oxide (NO_X) is considered one of the main gas pollutants for photochemical pollution, acid rain, and human asthma (Fang et al. 2020; Song et al. 2019). Fossil fuel combustion contributes in a great extent to the major anthropogenic source of NO_X (Rosas et al. 2012). At present, the main NO_X removal technologies are selective catalytic reduction (SCR), non-selective reduction, selective non-catalytic reduction (SNCR), and low NOx combustion technology (Zou et al. 2020; Ghosh et al. 2021; Cai et al. 2021; Song et al. 2021). The SCR for NO_X by ammonia over V_2O_5/TiO_2 is an effective denitration technology which is widely used in the temperature of 623.15–693.15 K (Liu et al. 2020). One of the major issues for SCR is that the technology is extremely inefficient at low temperatures. In order to solve the problem, removing NO_X from the low-temperature flue gas has been developed.

The possibility of using an activated carbon for NO_X removal from low-temperature flus gas has been broadly studied. MnO_X–CeO_2/carbon was synthesized and could promote the chemisorption of NO_X at 458.15 K (Cheng et al. 2021). Li et al. (2020) studied phosphorus-doped carbon aerogels in 373.15–473.15 K for reduction of NO_X. Qin et al. (2016) prepared $AO_x/CuO_y/C$ (A = Fe, Ni, Co, Mn), which showed the potential of low-temperature catalysis. Cai et al. (2016) developed the multi-layered Fe_2O_3@MnO_x@CNT catalyst, and the catalyst demonstrated outstanding low-temperature catalytic performance at 453.15–483.15 K. Busch et al. (2015) stabilized iron nanoparticles in carbon as a novel material to NO_X removal, and the material was not

Responsible Editor: George Z. Kyzas

Highlights
- The influence of the single and multiple factors on the catalyst was studied.
- The catalytic reduction process was described in a multi-principle-based way.
- The study provided information for the industrial applications.
- The catalyst was stable, environmentally friendly, and cost competitive.

✉ Weijun Zhang
zhangwj@smm.neu.edu.cn

[1] Industrial Furnace Research Institute, College of Metallurgy, Northeastern University, NO. 3-11, Wenhua Road, Heping District, Shenyang 110819, Liaoning, China

inactivated at 425 K, and NO_X was still removed at 328 K. The properties and applications of carbon-based materials are diverse. The porous graphene is non-hazardous, biocompatible, and stable and has excellent absorptive properties (Asiya et al. 2021; Panda et al., 2021). Some carbon-based iron materials were studied for use in the treatment of pollutants, such as heavy metals remediation and hazardous 4-nitrophenol reduction (Asif et al. 2021; Liang et al. 2022). In order to increase the low-temperature, NO_X conversion, noble metals, metal oxides, and transition metals were added to carriers (Qin et al. 2016; Chen et al. 2011, 2018; Choi et al. 2018; Wang et al. 2012; Zhang et al. 2015; Ye et al. 2020). Transition metal is considered to be a less expensive alternative, which is investigated by different authors. Fe, Mn, Fe_2O_3, CrO_3, and Co_3O_4 have been found to be capable of removing NO_X at low temperatures (Cao et al. 2015; Samojeden and Grzybek 2016; Wang et al. 2016; Bai et al. 2019). Iron is often used as an active component of denitrification catalysts because of its low price, non-toxicity, and abundant (Zhou et al. 2017; Yuan et al. 2017). Lu et al. (2018) found that the NO_X removal efficiency was more than 70% by the activated coke loaded with 3% $Fe_{0.6}Co_{0.2}Ce_{0.2}O_{1.57}$ at 373.15 K. Fang et al. (2017) studied $Fe_{0.3}Mn_{0.5}Zr_{0.2}$ catalyst and achieved an excellent denitration performance, and the NO_X conversion was 100% at 473.15–633.15 K. Other iron oxides catalysts, like $Fe_{0.7}Mn_{0.15}Mg_{0.15}O_Z$, Fe/Cu-SAPO-34, and iron-niobium composite oxides, were also deeply investigated (Zhang et al. 2017a, b; Zhang and Yang 2017; Zhang et al. 2017a, b). In the past, the low-temperature modification of catalysts has been studied, but there is a little literature data available about kinetics of the transition metal on carbon. In addition, compared with the previous study, the NO_X removal process of C-ZFe was discussed. C-ZFe did not produce secondary pollution, the raw materials were widely sourced, and the preparation method was simple, which were suitable for industrial applications.

In the present paper, the zero iron was loaded on the activated carbon and was employed to NO_X removal (nitrous oxide is a general name of a class of compounds, and NO was used as the representative of the study) at low temperatures. The performance tests of multiple factors on NO_X conversion were carried out. The physical and chemical properties of the catalysts were studied by SEM–EDS, surface area and pore size distribution measurements, XRD, and XPS. The kinetics at the low temperatures were studied, which could provide information for industrial parameter and supplement the blank of research data.

The aim of this work was to study the kinetics for NO_X reduction on the carbon-based zero valent iron catalyst. The experimental results were correlated with a kinetic model that represented adequately these experimental data. The kinetic parameters of rate constant, reaction order, and apparent activation energy were obtained for understanding the process of NO_X reduction and for designing the reactor.

Materials and methods

Materials: catalyst preparation

The carbon powder and iron ore powder (Boliante Metallurgical Technology Co. Ltd., China) were used to synthetic C-ZFe catalyst. A total of 15 wt.% carbon powder and 85 wt.% iron ore powder were put into the star wheel mixer mixing and rolling. The raw pellets with diameter of 12–18 mm were formed by the disk-type pelletizing machine. Then the pellets were dried at 383.15 K for using (the water content was controlled below 5%). The dried pellets were put into can and calcined in a shuttle kiln at 1323.15 K for 8–10 h. After calcining, the pellets were cooled down to room temperature as C-ZFe catalyst.

Methods

In order to capture the characteristics of the surface of the sample, the samples were observed by scanning electron micrograph (SEM), ULTRA PLUS, and Zeiss microscope (Germany) co. LTD. Energy dispersive spectroscopy (EDS) was used for elemental analysis in conjunction with SEM. The surface scanning method was used to analyze the composition of microregion qualitatively and semi-quantitatively.

Surface area and pore size distribution measurements were measured by N_2 adsorption isotherm at 77 K using Micromeritics 3H-2000PS1. The specific surface area was calculated by the Brunauer, Emmet, and Teller (BET) model. The pore structure parameters were obtained via Barrett, Joyner, and Halenda (BJH) model.

X-ray diffraction (XRD) patterns were obtained by Panaco (Netherlands) equipped with a Cu tube serving as the X-ray source. It was employed to determine the crystal phase and dispersion of the iron particles on the carbon support. The powdered samples were pressed onto suitable holders and scanned within the 2θ range 10–90° with a 0.02 step length.

The X-ray photoelectron spectroscopy (XPS) analysis was performed using Al K alpha source with a Scienta SES 2002 spectrometer operating at constant transmission energy ($Ep = 30$ eV). The results of the analyses were all corrected with C1s.

Experiment: catalytic performance measurement

The tests were carried out in a fixed-quartz reactor (200 cm high with a diameter of 5 cm) connected to a flue gas analyzer. The flue gas analyzer (England flue gas analyzer, Kane 9206) was used for analyzing the concentrations

of the import and export NO_X, so that the conversion of NO with C-ZFe catalyst could be measured. The resistance furnace could effectively control the temperatures (398.15 K, 403.15 K, 408.15 K). A stainless-steel plate with holes were placed at the bottom of the reactor to prevent pellets from falling off and clogging the pipeline. A measured amount of C-ZFe catalyst was placed in the reactor. C-ZFe was purged in situ by passing Ar for 30 min at the reaction temperature before each test. The tests of kinetics were performed with a mixture of NO (350 ppm, 550 ppm, 750 ppm) and O_2 (15 vol%) balanced by Ar, which the total intake flow was 21 L/min. The flow rate of various gases was controlled by mass flow meters (Senvenstar, D07-19B and D07-9E). Figure 1 shows the system diagram for the performance tests of the catalyst. The NO conversion was calculated according to Eq. (1):

$$\text{NO conversion} = \frac{C_{\text{NOinlet}} - C_{\text{NOoulet}}}{C_{\text{NOinlet}}} \times 100\% \quad (1)$$

Among which, NO_{inlet} is the concentration of nitric oxide (NO) at the inlet of the reactor, and NO_{outlet} is the concentration of NO at the outlet of the reactor.

Results and discussion

As shown in Fig. 2a, pore structures exist on the surface of the catalyst. According to the classification of pores by the International Union of Theoretical and Applied Chemistry (IUPAC), pores larger than 50 nm are macropores, pores smaller than 2 nm are micropores, and those in between are mesopores. The pore size of the catalyst in Fig. 2b is 6.49 nm, and its surface structure is mainly mesoporous. In addition, as shown in Fig. 2c and d, the iron and the carbon are distributed on the surface of the catalyst. According to the mass content of surface elements in Fig. 2a, C is 12.91 wt.% and Fe is 67.83 wt.%. It can be seen that the preparation method of the catalyst almost achieved the expected goal (catalyst preparation: 15 wt.% carbon powder and 85 wt.% iron ore powder).

Figure 3 shows the XRD patterns of C-ZFe catalyst before and after denitration. It can be seen that the phase composition did not change before and after denitration. Both of the samples showed the main diffraction peaks corresponded to Fe ((ICDD PDF NO. 06–0696, Massa 2014), at 2-theta 44.7, 65.0, and 82.3. The diffraction peaks at 2-theta 34.2, 35.7, and 60.2 were the characteristic diffraction peaks of SiC (ICDD PDF NO. 29–1131, Massa 2014).

The higher peak intensity at 2-theta 44.7 and 82.3 for the catalysts indicated that the (110) and (211) planes were the main exposed crystal planes. For SiC, which was a small amount of impurity in the materials, the peak intensity was relatively weak. In addition, the relative intensity of Fe on C-ZFe catalyst after denitration was obviously stronger than that before denitration. It is well known that the relative intensity is determined by the diffraction capacity of the phase. Specifically, the relative content of the phase, the dispersion, and the grain size that all affect the diffraction

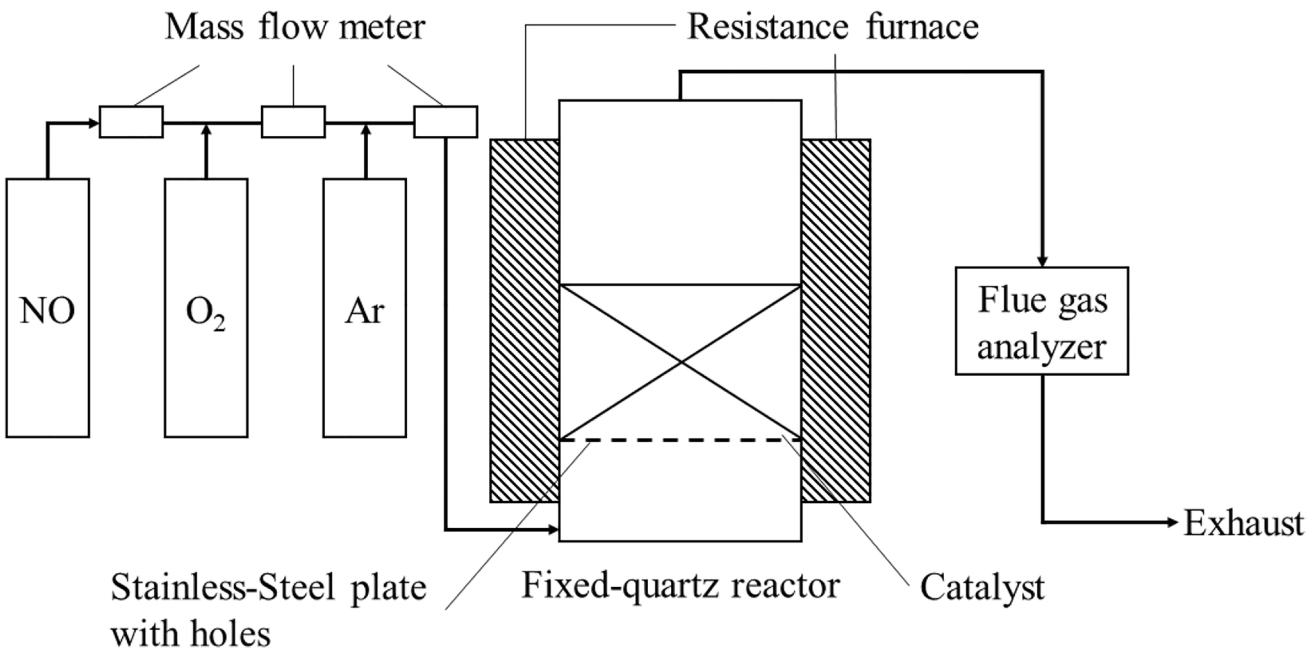

Fig. 1 System diagram

ability (Jin et al. 2020; Liu et al. 2020; Zhang et al. 2020). According to the testing process of C-ZFe catalyst and the results in Fig. 3, the peak sharpness and half peak width of Fe have no obvious change. Therefore, the change of iron grain was not enough to cause such a variation in the relative intensity, and it was mainly the relative content or the dispersion that affected the intensity. In order to explore the above substances, we further carried out quantitative analysis of C, Fe, and other elements.

According to the semi-quantitative analysis of XPS test in Table 1, compared with the data of C atom at 298.15 K and 408.15 K, the relative content of C atom after denitration at 408.15 K decreased significantly. On the one hand, the difference in atomic percentage indicated that the mechanism of denitration at room temperature was different from that at the low temperature (408.15 K). On the other hand, it indicated that carbon was consumed for redox reaction at 408.15 K. Some studies have shown that the carbon participated in redox reactions with NO to produce N_2, N_2O, CO, and CO_2 (Teng and Suuberg 1993; Nishi et al. 1997; Alcañiz-Monge et al. 2008), which were consistent with the results of this study. Combined with the results in Fig. 3, the iron peak was enhanced after denitrification, which was also because the relative content of iron increased after the carbon consumption.

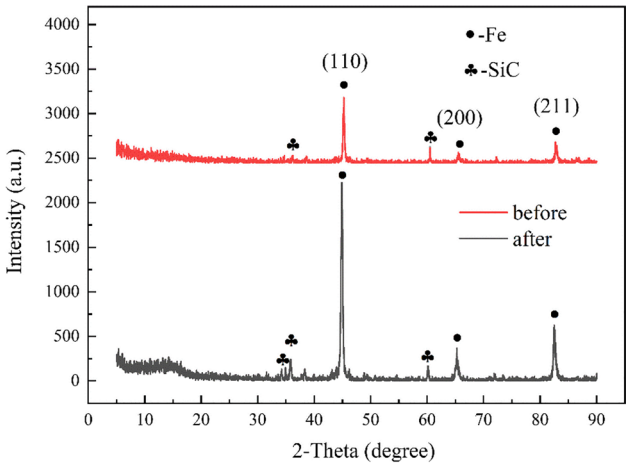

Fig. 3 XRD patterns of C-ZFe before and after denitration

Interactive effect of multiple factors

Box-behnken experimental design (BBD) method was used to take NO_X conversion as the response value. Temperature (398.15 K, 403.15 K, and 408.15 K), concentration of NO (350 ppm, 550 ppm, and 750 ppm), and bed height (80 cm, 110 cm, and 140 cm) were selected as three factors for the tests. In order to simplify the design, the values of each

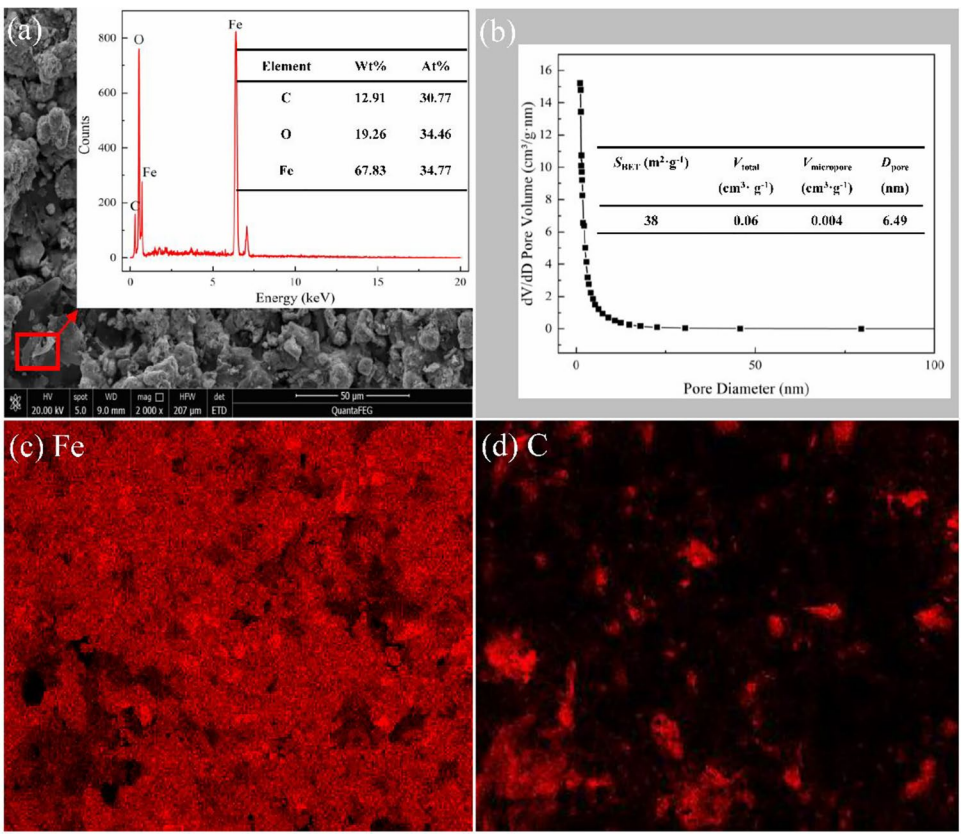

Fig. 2 EDS surface scanning and BJH pore diameter distributions of the catalyst. **a** SEM micrograph, **b** BJH pore diameter distributions, **c** EDS surface scanning results of Fe, **d** EDS surface scanning results of C

Table 1 Surface elemental content of C-ZFe after denitrification at room temperature and 408.15 K

Element	Percentage of each atom in catalyst (%)	
	298.15 K	408.15 K
C	90.47	79.39
N	0.94	1.31
O	7.26	15.10
Fe	1.34	4.20

factor need to be standardized, that was, the upper level corresponded to 1, the lower level was − 1, and the zero level was 0. Table 2 shows the encoding and level of each factor. The Design Expert 8.0.6 software was used to design the experiments and achieved the interactive effect of factors. Table 3 shows the results of the BBD design.

The data in Table 3 were processed by the Design Expert 8.0.6 software, and the quadratic regression equation of NO_X conversion, variance analysis (Table 4), and the accuracy of the model (Table 5) can be obtained:

$$Y = 45.6 + 1.69B + 16.26C + 0.8AB + 1.45AC + 1.38BC + 0.21A^2 - 0.61B^2 + 7.59C^2 \quad (2)$$

From Table 4, the F value of the model is 104.32, indicating that the model was very significant and there was only 0.01% probability that secondary factors would affect the response value. Model $P < 0.0001$, indicating that the experimental error was small, and uncontrolled factors had minimal interference to the experimental results. From Table 5, R^2 is 0.99, indicating that the model can reasonably explain 99% of the experimental data, and the fitting degree was good. In addition, it can be seen from Table 4 that the order of influence degree of each factor on response value is as follows: C > B > A; AC is as significant as BC, but both are more significant than AB. This was consistent with the results in Fig. 4. The response surface in Fig. 4a shows no significant fluctuation, indicating that temperature and concentration of NO had no significant influence on NO_X conversion (combined with the results of single factors, the combination of A and B was two less significant single factors' combination, so it was indeed less significant in the interaction influence). According to Fig. 4b and c, the interaction influence of AC was as significant as BC. What's more, high NO_X conversion area (red area) appears, which also indicated that bed height was the factor that had the greatest influence on the response value. Therefore, the optimal process parameters were determined as follows: the bed height was 140 cm (the space velocity was 459 h^{-1}), the temperature was 408.15 K, the concentration of NO was 550 ppm. At the conditions, the NO_X conversion was 72.7% and the kinetics of gas–solid catalytic reaction would be further studied.

Table 2 Encoding and level of each factor

Level	Factor		
	A. Temperature/K	B. Concentration of NO/ppm	C. Bed height/cm
− 1	398.15	350	80
0	403.15	550	110
1	408.15	750	140

Table 3 BBD design and standardization results

Order	A	B	C	Y. NO_X conversion and standard deviation/%
1	0	0	0	47.1 ± 1.11
2	0	0	0	45.0 ± 1.06
3	− 1	0	1	67.2 ± 1.06
4	1	1	0	46.5 ± 1.15
5	0	1	1	71.5 ± 1.20
6	− 1	0	− 1	37.0 ± 1.11
7	1	0	1	72.7 ± 1.21
8	− 1	1	0	47.5 ± 1.15
9	0	− 1	− 1	36.4 ± 1.15
10	0	1	− 1	36.8 ± 1.11
11	1	0	− 1	36.7 ± 1.06
12	0	0	0	46.0 ± 1.00
13	0	− 1	1	65.6 ± 1.04
14	0	0	0	44.9 ± 1.21
15	0	0	0	45.0 ± 1.00
16	− 1	− 1	0	45.5 ± 1.05
17	1	− 1	0	41.3 ± 1.08

Table 4 Variance analysis

Project	*F*	*P*	Significance
Model	104.32	< 0.0001	**
A	$1.78 \times 10.^{-13}$	1	
B	8.91	0.02	*
C	827.27	< 0.0001	**
AB	1.00	0.35	
AC	3.29	0.11	
BC	2.96	0.13	
$A.^2$	0.07	0.79	
$B.^2$	0.62	0.46	
$C.^2$	94.78	< 0.0001	**

$^{**}p < 0.01$; $^{*}0.01 < p < 0.05$

Discussion on the mechanism of NO removal reaction

The results described above enable to propose a kinetic rate law for removal of NO by C-ZFe at a low temperature. Based on the catalysts process of L–H and Mars Van Krevelen mechanism (Chen and Jiu 2011; Bai and Liu 2015), the flowing reactions took place on the surface and inner hole of the catalyst:

$$\mathrm{NO} + \sigma_{\mathrm{ads}} \underset{k_{\mathrm{dNO}}}{\overset{k_{\mathrm{aNO}}}{\Leftrightarrow}} \mathrm{NO}\sigma_{\mathrm{ads}}\ (\mathrm{L-H\ mechanism}) \tag{3}$$

$$\mathrm{NO}\sigma_{\mathrm{ads}} + \mathrm{C}\sigma_{\mathrm{red}} \overset{k_s}{\Rightarrow} \mathrm{N_2}\sigma_{\mathrm{ads}} + \mathrm{CO_2}\sigma_{\mathrm{ox}}\ (\mathrm{Mars\ Van\ Krevelen\ mechanism}) \tag{4}$$

$$\mathrm{N_2}\sigma_{\mathrm{ads}} \underset{k_{\mathrm{aN_2}}}{\overset{k_{\mathrm{dN_2}}}{\Leftrightarrow}} \mathrm{N_2} + \sigma_{\mathrm{ads}}\ (\mathrm{L-H\ mechanism}) \tag{5}$$

$$\mathrm{CO_2}\sigma_{ox} \underset{k_{aCO_2}}{\overset{k_{dCO_2}}{\Leftrightarrow}} \mathrm{CO_2} + \sigma_{\mathrm{ox}}\ (\mathrm{L-H\ mechanism}) \tag{6}$$

Based on the single-molecule L–H kinetic model, there are active sites on the surface of the catalyst, and a reactant is adsorbed on the uniform surface of the catalyst and can be adsorbed in only one layer. In addition, according to the Mars van Krevelen kinetic model, many catalytic reactions take place by redox mechanism, which should include active sites of oxidation state and reduction state. In summary, there were three types of active sites on C-ZFe catalyst, which were the reduction active site that could occur redox reaction, the active site that could not occur redox reaction (adsorption site) and the empty active site. The adsorption site could absorb NO, and the adjacent reduced active site would react with the adsorbed NO and generate adsorbed N_2 and oxidized CO_2 (equivalented to the adsorbed CO_2, details were given below). Finally, N_2 and CO_2 were desorbed from the site.

It is generally believed that the rate of surface reaction is slower than that of adsorption, so the surface reaction process (4) was taken as the rate-limiting step. In addition, nitrogen is an inert gas and the experimental results showed that the amount of CO_2 was very small, so the reverse reaction can be ignored. The total reaction rate is expressed as:

$$r = k_s \theta_{\mathrm{NO}} \theta_{\mathrm{red}} \tag{7}$$

where r represents the NO_X conversion rate of the catalyst, mol/(g·min); k_s represents the reaction rate constant, L/(g·min); θ_{red} and θ_{NO} are the coverage of reactant NO at the reduction active site and adsorption site respectively.

Table 5 Analysis of the model

Standard deviation	Mean value	Coefficient of dispersion (%)	R^2
1.60	48.98	3.26	0.99

According to the steady-state approximation principle, Eqs. (3), (5), and (6) are balanced:

$$k_{\mathrm{aNO}} P_{\mathrm{NO}} \theta_{\mathrm{V}} = k_{\mathrm{dNO}} \theta_{\mathrm{NO}}\ or\ \theta_{\mathrm{NO}} = \frac{k_{\mathrm{aNO}}}{k_{\mathrm{dNO}}} P_{\mathrm{NO}} \theta_{\mathrm{V}} = K_{\mathrm{NO}} P_{\mathrm{NO}} \theta_{\mathrm{V}} \tag{8}$$

$$k_{\mathrm{dN_2}} \theta_{\mathrm{N_2}} = k_{\mathrm{aN_2}} P_{\mathrm{N_2}} \theta_{\mathrm{V}}\ or\ \theta_{\mathrm{N_2}} = \frac{k_{\mathrm{aN_2}}}{k_{\mathrm{dN_2}}} P_{\mathrm{N_2}} \theta_{\mathrm{V}} = K_{\mathrm{N_2}} P_{\mathrm{N_2}} \theta_{\mathrm{V}} \tag{9}$$

$$k_{\mathrm{dCO_2}} \theta_{\mathrm{CO_2}} = k_{\mathrm{aCO_2}} P_{\mathrm{CO_2}} \theta_{\mathrm{V}}\ or\ \theta_{\mathrm{CO_2}} = \frac{k_{\mathrm{aCO_2}}}{k_{\mathrm{dCO_2}}} P_{\mathrm{CO_2}} \theta_{\mathrm{V}} = K_{\mathrm{CO_2}} P_{\mathrm{CO_2}} \theta_{\mathrm{V}} \tag{10}$$

where θ_{N_2}, θ_{CO_2}, and θ_V are the coverage of adsorption site of N_2, CO_2, and empty active site of C-ZFe catalyst respectively. Here, it was necessary to explain the reason why the oxidation active site was classified as adsorption site in Eq. (6). According to the previous thermodynamic analyses (Cao and Zhang 2020) and experimental results above, the generation of CO_2 was based on the chemical reaction process of carbon reduction, rather than the role played by the active site. Therefore, L–H mechanism was followed and Eq. (10) was given accordingly. In addition, CO_2 was released from the oxidation active site, and the oxidation active site did not further participate in further reaction. This process was very similar to Eq. (5), and the role of the oxidation active site and adsorption site was analogical.

$$\theta_{\mathrm{red}} + \theta_{\mathrm{NO}} + \theta_{\mathrm{N_2}} + \theta_{\mathrm{CO_2}} + \theta_{\mathrm{V}} = 1 \tag{11}$$

Substitute Eqs. (8), (9), and (10) into (11):

$$\theta_{\mathrm{V}} = \frac{1 - \theta_{\mathrm{red}}}{1 + K_{\mathrm{NO}} P_{\mathrm{NO}} + K_{\mathrm{N_2}} P_{\mathrm{N_2}} + K_{\mathrm{CO_2}} P_{\mathrm{CO_2}}} \tag{12}$$

Substitute Eq. (12) into (8), (9), and (10) respectively:

$$\theta_{\mathrm{NO}} = \frac{K_{\mathrm{NO}} P_{\mathrm{NO}} (1 - \theta_{\mathrm{red}})}{1 + K_{\mathrm{NO}} P_{\mathrm{NO}} + K_{\mathrm{N_2}} P_{\mathrm{N_2}} + K_{\mathrm{CO_2}} P_{\mathrm{CO_2}}} \tag{13}$$

$$\theta_{\mathrm{N_2}} = \frac{K_{\mathrm{N_2}} P_{\mathrm{N_2}} (1 - \theta_{\mathrm{red}})}{1 + K_{\mathrm{NO}} P_{\mathrm{NO}} + K_{\mathrm{N_2}} P_{\mathrm{N_2}} + K_{\mathrm{CO_2}} P_{\mathrm{CO_2}}} \tag{14}$$

$$\theta_{\mathrm{CO_2}} = \frac{K_{\mathrm{CO_2}} P_{\mathrm{CO_2}} (1 - \theta_{\mathrm{red}})}{1 + K_{\mathrm{NO}} P_{\mathrm{NO}} + K_{\mathrm{N_2}} P_{\mathrm{N_2}} + K_{\mathrm{CO_2}} P_{\mathrm{CO_2}}} \tag{15}$$

Substitute Eqs. (13), (14), and (15) into (7):

$$r = \frac{k_s K_{\mathrm{NO}} P_{\mathrm{NO}} \theta_{\mathrm{red}} (1 - \theta_{\mathrm{red}})}{1 + K_{\mathrm{NO}} P_{\mathrm{NO}} + K_{\mathrm{N_2}} P_{\mathrm{N_2}} + K_{\mathrm{CO_2}} P_{\mathrm{CO_2}}} \tag{16}$$

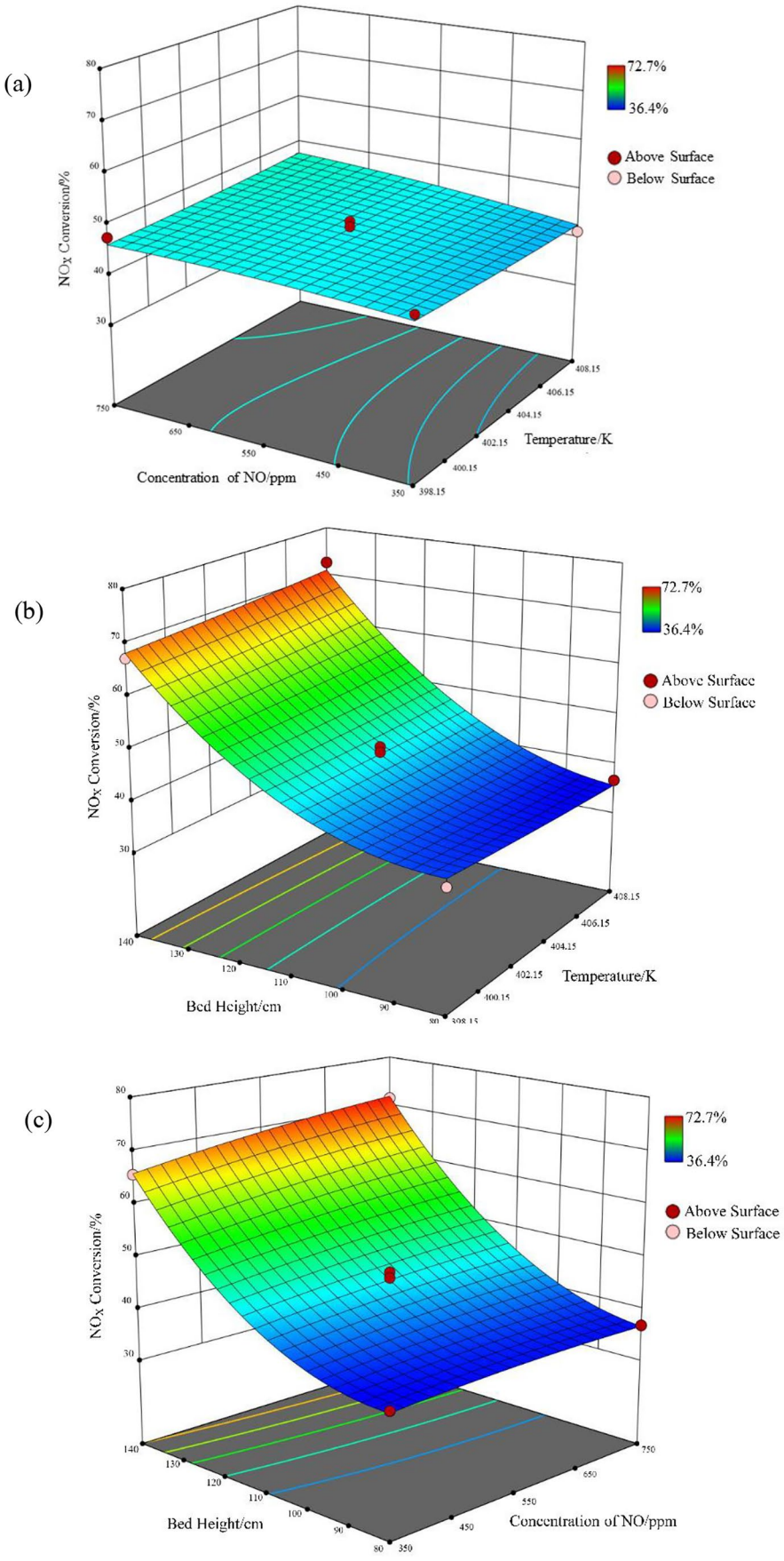

Fig. 4 Interaction of multiple factors on NO_X conversion. **a** temperature and NO concentration, **b** catalyst bed height and temperature, **c** catalyst bed height and concentration of NO

According to Eq. (16), it can be concluded that the reaction rate in the low-temperature denitration reaction process of C-ZFe catalyst is determined by P_{NO} and θ_{red}. In addition, the larger the load of zero-valent iron was not the better, too much load would block the mesopore and reduced the adsorption capacity. The load of zero-valent iron had the best value, which was directly related to the load. In other words, θ_{red} can be incorporated into the constant term.

In general, when only the effect of reactants on the reaction rate is considered, simplification (16):

$$r = \frac{k_s' K_{NO} P_{NO}}{1 + K_{NO} P_{NO}} \tag{17}$$

According to Eq. (17), when the reactant NO is weakly adsorbed ($K_{NO}P_{NO} \ll 1$) on the catalyst, this reaction is a quasi-first-order reaction. In order to verify the above conclusions, the catalytic reaction kinetics experiments were carried out at different temperatures (398.15 K, 403.15 K, and 408.15 K).

According to the quasi-first-order kinetic model:

$$-\frac{dC_{NO}}{dt} = k_1 C_{NO} \tag{18}$$

where dC_{NO} is the concentration of NO when dt, ppm; C_{NO} is the concentration of NO at time t, ppm; and k_1 is the reaction rate constant, min^{-1}.

Integral and linearization:

$$\int_{C_{NO,0}}^{C_{NO}} \frac{1}{C_{NO}} dC_{NO} = \int_0^t -k_1 dt \tag{19}$$

$$C_{NO} = C_{NO,0} \cdot e^{-k_1 t} \tag{20}$$

$$\ln \frac{C_{NO}}{C_{NO,0}} = -k_1 t \tag{21}$$

$$\ln C_{NO} = \ln C_{NO,0} - k_1 t \tag{22}$$

The experiment was carried out at the experimental conditions with optimal operation parameters. The first-order kinetic model was only applicable to the initial stage of a kinetic description, therefore, the results that from 0 to 30 min in the initial stage of experiments were selected for analyses. According to Eq. (22), $\ln C_{NO}$ was plotted against t to obtain catalytic kinetic curves at different temperatures, as shown in Fig. 5. The kinetic parameters of C-ZFe catalyst are shown in Table 6.

Figure 5 shows the gas–solid catalytic kinetic curve of NO removal over C-ZFe catalyst. In Fig. 5, the red curve is the simulated value of the first-order kinetic model, and the black square is the actual experimental value. It can be seen from the trend of simulated values and actual values that they have a high degree of fitting, and $\ln C_{NO}$ to t is the linear at the three experimental temperatures. In addition, it can be seen from R^2 in Table 6 that the reliability of this experiment is high, that is, 99% of the data at 398.15 K and the reliability is higher than 98% at 403.15 K and 408.15 K. This indicated that the gas–solid catalytic kinetic process of the NO removal by C-ZFe at a low temperature was a quasi-first-order kinetic reaction. Qi and Yang (2003) and Wu et al. (2007) studied the kinetics of NH_3-SCR by using power function, and the results showed that the reaction order was one (NO was one, and NH_3 was zero), which was consistent with the results of this study.

The relationship between the reaction rate constant and the temperature conforms to Arrhenius equation, which is expressed as follows:

$$k = A \exp\left(-\frac{E_c}{RT}\right) \tag{23}$$

where A is the pre-exponential factor, min^{-1}; E_c is the activation energy, kJ/mol; R is the gas constant, the value is 8.314×10^{-3} kJ/(mol·K); T is the absolute temperature, K.

Taking the logarithm of Eq. (23) and giving a linear equation of $\ln k$ with to $1/T$:

$$\ln k = -\frac{E_c}{R} \cdot \frac{1}{T} + \ln A \tag{24}$$

As shown in Fig. 6, the linear equation of $\ln k$ to $1/T$ is obtained according to the linear fitting curve, and the slope and intercept of the equation were obtained. The above parameters were substituted into Eq. (24), the activation energy was 41.57 kJ/mol, and the pre-exponential factor was 2980 min^{-1}.

Prediction and modeling of De-NO_X activity

The relationship between the reaction rate and NO conversion rate can be obtained according to the kinetic study above. Therefore, a De-NO_X reactor can be designed at a given conversion rate or specified operating conditions. Meanwhile, the simulation calculation at any conditions was carried out, which provided valuable information for the design of pilot scale reactor.

For the present catalytic system, if the fixed-quartz reactor is regarded as an ideal plug flow reactor (PFR), the integral form of the design rate equation of the reactor is:

$$V_R = V_0 C_{NO} \int_0^X \frac{d_{X_{NO}}}{r_{NO}} \tag{25}$$

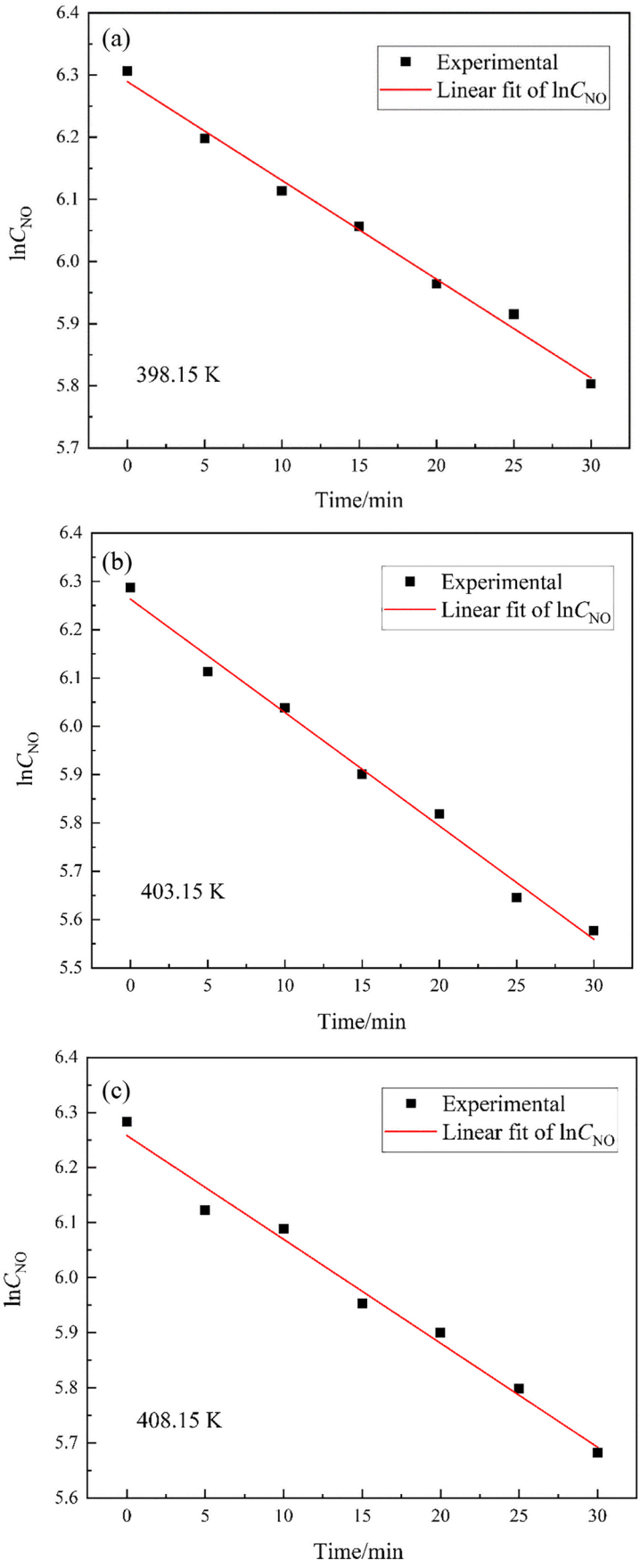

Fig. 5 Kinetic curves of gas–solid catalysis at different temperatures. **a** 398.15 K, **b** 403.15 K, **c** 408.15 K

Table 6 Kinetic parameters

Reaction temperature (K)	Reaction rate constant (min^{-1})	R^2
398.15	0.016	0.990
403.15	0.019	0.982
408.15	0.024	0.988

where V_R is the reaction volume, L; V_0 is the volume flow, L/min; C_{NO} is the initial concentration of NO; X is the conversion rate of NO, %; r_{NO} is the reaction rate equation of NO and it was obtained by above.

$$r_{NO} = k \cdot C'_{NO} \tag{26}$$

Further neglecting the pressure drop through the channel and treat the simulated gas as an ideal gas, the contact (reaction) time t can be expressed by introducing the temperature correction:

$$\tau = \frac{V_R}{V_0} = \frac{L \cdot S \cdot T_0}{V_0 \cdot T} \tag{27}$$

where τ is reaction time, min; L is the length of the catalyst (the stacking shape was a cylinder), m; S is the base area of catalyst, m^2; T_0 is equal to 273 K and T is the reaction temperature, K. Combining Eqs. (25), (27), and (26), the expression of the NO conversion rate and contact time is obtained:

$$\begin{aligned}\tau &= C_{NO}\int_0^X \frac{1}{k \bullet C'_{NO}} d_X \\ &= \frac{1}{k}\int_0^X \frac{1}{C'_{NO}/C_{NO}} d_X \\ &= \frac{1}{k}\int_0^X \frac{1}{1-X} d_X \\ &= -\frac{1}{k}\ln(1-X)\end{aligned} \tag{28}$$

After sorting and simplifying Eq. (28), the following can be obtained:

$$X = 1 - e^{-k\tau} \tag{29}$$

The relationship between reaction rate constant, NO conversion rate, and catalyst length are obtained by using Eqs. (27) and (29):

$$\mathrm{k} = -\frac{\ln(1-\mathrm{X}) \cdot \mathrm{V_0} \cdot \mathrm{T}}{\mathrm{L} \cdot \mathrm{S} \cdot \mathrm{T_0}} \tag{30}$$

The relationship between the reaction rate constant and temperature generally obeys the Arrhenius equation:

$$k = A\exp(-\frac{E}{RT}) \tag{31}$$

$$\ln\ k = \ln\ A - \frac{E}{RT} \tag{32}$$

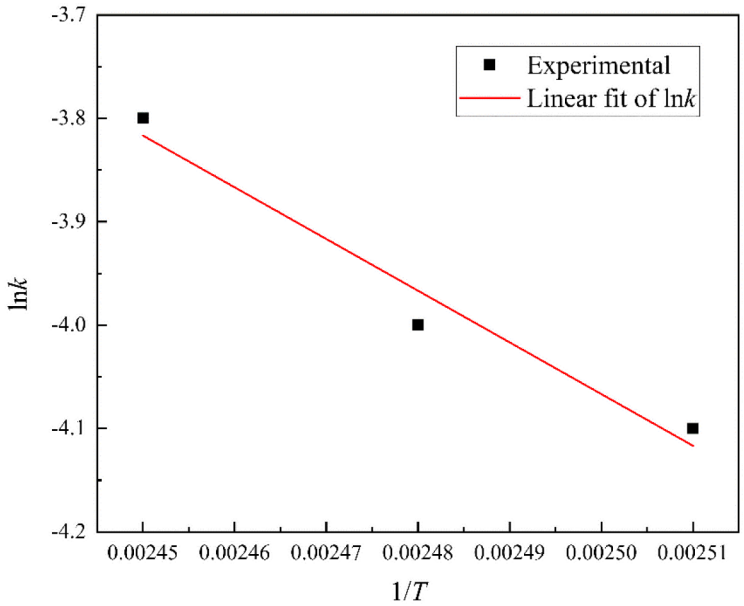

Fig. 6 ln$k$ varies with 1/T

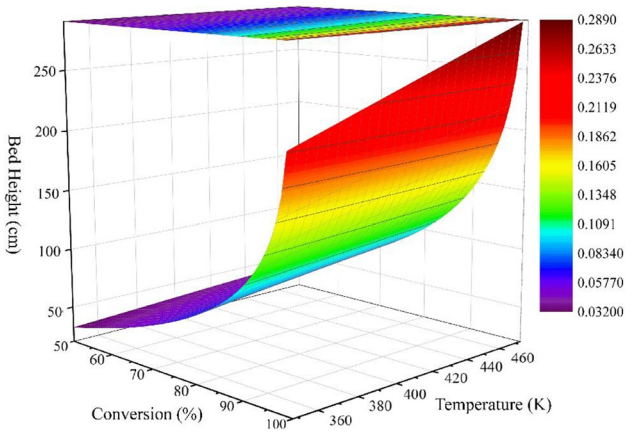

Fig. 7 Response surface of NO conversion with design reaction temperatures and the catalyst bed height

where A refers to the pre-exponential factor, min^{-1}; E is the apparent activation energy, J/mol; R is the gas constant, 8.314 J/(mol·K); T is the reaction temperature.

Further combining Eqs. (30) and (32) then gives:

$$X = 1 - e^{-\frac{A \cdot L \cdot S \cdot T_0}{V_{NO} \cdot T} \times e^{-\frac{E}{RT}}} \quad (33)$$

According to the above kinetic calculation of the gas–solid catalytic reaction, A is 2980 min^{-1} and E is 41.57 J/mol. Substitute the above data into Eq. (33). In addition, according to the characteristics of low-temperature flue gas and the C-ZFe catalyst, the Eq. (33) was processed by Origin software to obtain the response surface of the reactor design of C-ZFe catalyst. The results are shown in Fig. 7.

Figure 7 displays the simulated NO conversion as a function of the set of reaction temperatures and the length of the catalyst (bed height), which is surely helpful for the design of pilot-plant scale SCR De-NO_X reactors. For example, when the catalyst is applied in a given scenario where the general temperature condition and the expected conversion rate are determined according to the industry emission standard, the minimum amount of the catalyst can be obtained from Fig. 7. Also, the minimum volume of the reactor can be determined.

Conclusions

Removal NO_X by C-ZFe at low-temperature conditions is a method that is environmentally friendly. C-ZFe materials are widely available and the synthesis method is simple, which is cost competitive and has the potential of an industrial application. In the present study, catalyst performance experiments were carried out in a fixed-quartz reactor. The physicochemical properties were investigated by SEM–EDS, surface area and pore size distribution measurements, XRD, and XPS. BBD experimental design was used to study the interaction of operating parameters. The results showed that the order of the influence of single factor on NO_X conversion was catalyst bed height > concentration of NO > temperature; among the interaction effects of multiple factors, the interaction effect of temperature and catalyst bed height, NO concentration, and catalyst bed height was more significant. The optimal operating conditions were as follows: the catalyst bed height was 140 cm, the temperature was 408.15 K, the concentration of NO was 550 ppm, under which the NO_X conversion was 72.7%. In addition, based on L–H and Mars van Krevelen mechanism, the kinetics of low-temperature denitrification over C-ZFe catalyst was studied. It was found that the reaction conformed to the quasi-first order kinetic model. According to the Arrhenius equation, kinetic parameters were obtained as the apparent activation energy was 41.57 kJ/mol and the pre-exponential factor was 2980 min^{-1}. By the reaction rate equation and kinetic parameters obtained from the kinetic research, the De-NO_X reactor was designed, which could provide valuable information for the design of pilot reactors.

Acknowledgements The authors are grateful to Guangyang Xie and Huiqiang Wang for the contribution to the preliminary experimental work.

Author contribution Weijun Zhang gave the idea and approved the final version. Wan Cao and Ziyang Guo analyzed the data and wrote the complete paper.

Funding This work was supported by the National Key Research and Development Program of China (project number 2017YFA0700300).

Data availability The datasets and materials used during the current study are available from the corresponding author on reasonable request.

Declarations

Ethics approval Not applicable.

Consent to participate I am free to contact any of the people involved in the research to seek further clarification and information.

Consent for publication Not applicable.

Competing interests The authors declare no competing interests.

References

Alcañiz-Monge J, Bueno-López A, Lillo-Rodenas MÁ, Illán-Gómez MJ (2008) NO adsorption on activated carbon fibers from iron-containing pitch. Micropor Mesopr Mat 108:294–302

Asif I, Baig N, Sher M, UI-Hamid A, Altaf M, Mumtaz A, Sohail M (2021) MOF derived novel zero-valent iron @ graphitic

carbon-based nanoreactors for selective reduction of hazardous 4-nitrophenol. Clean Eng Technol 2:100081
Asiya SI, George ZK, Kaushik P, Fernando GDSJ (2021) Graphene functionalized hybrid nanomaterials for industrial-scale applications: a systematic review. J Mol Struct 1239:130518
Bai TC, Liu F (2015) Physical and chemical. Bai, Nanjing
Bai YR, Dong JP, Hou YQ, Guo YP, Liu YJ, Li YL, Han XJ, Huang ZG (2019) Co_3O_4@PC derived from ZIF-67 as an efficient catalyst for the selective catalytic reduction of NO_X with NH_3 at low temperature. Chem Eng J 361:703–712
Busch M, Kompch A, Suleiman S, Notthoff C, Bergmann U, Theissmann R, Atakan B, Winterer M (2015) NO_X conversion properties of a novel material: Iron nanoparticles stabilized in carbon. Appl Catal B Environ 166–167:211–216
Cai J, Zheng W, Wang Q (2021) Effects of hydrogen peroxide, sodium carbonate, and ethanol additives on the urea-based SNCR process. Sci Total Environ 772:145551
Cai S, Hu H, Li H, Shia L, Zhang D (2016) Design of multi-shell Fe_2O_3@$MnO_{(x)}$@CNTs for the selective catalytic reduction of NO with NH_3: improvement of catalytic activity and SO_2 tolerance. Nanoscale 8:3588–3598
Cao F, Su S, Xiang J, Wang P, Hu S, Sun L, Zhang A (2015) The activity and mechanism study of Fe–Mn–Ce/γ-Al_2O_3 catalyst for low temperature selective catalytic reduction of NO with NH_3. Fuel 139:232–239
Cao W, Zhang WJ (2020) Low temperature selective catalytic reduction of nitric oxide with an activated carbon-supported zero-valent iron catalyst. Rsc Adv 10:42613–42618
Chen SY, Jiu JY (2011) Engineering foundation of catalytic reaction. Cheng, Beijing
Chen J, Zhu B, Sun Y, Yin S, Zhu Z (2018) Investigation of low-temperature selective catalytic reduction of NO_X with ammonia over Mn-modified Fe_2O_3/AC catalysts. J Brazil Chem Soc 1:79–87
Chen Z, Wang F, Li H, Yang Q, Wang L, Li X (2011) Low-temperature selective catalytic reduction of NO_X with NH_3 over Fe–Mn mixed-oxide catalysts containing $Fe_3Mn_3O_8$ phase. Ind Eng Chem Res 51:202–212
Cheng XM, Xiao XX, Yin Y, Wang JT, Qiao WM, Ling LC (2021) Ammonia-free selective catalytic reduction of NO at low temperature on melamine impregnated MnOx–CeO_2/carbon aerogels. Ind Eng Chem Res 60:13233–13242
Choi CH, Lim HK, Chung MW, Chon G, Sahraie NR, Altin A, Sougrati MT, Stievano L, Oh HS, Park ES, Lou F, Strasser P, Dražić G, Mayrhofer KJJ, Kim H, Jaouen F (2018) The Achilles' heel of iron-based catalysts during oxygen reduction in an acidic medium. Energ Environ Sci 11:3176–3182
Fang N, Guo J, Shu S, Luo H, Chu Y, Li J (2017) Enhancement of low-temperature activity and sulfur resistance of $Fe_{0.3}Mn_{0.5}Zr_{0.2}$ catalyst for NO removal by NH_3-SCR. Chem Eng J 325:114–123
Fang X, Liu YJ, Cen WG, Cheng Y (2020) Birnessite as a highly efficient catalyst for low-temperature NH_3-SCR: the vital role of surface oxygen vacancies. Ind Eng Chem Res 59:14606–14615
Ghosh RS, Michael PH, Wang D (2021) Selective oxidation of NH_3 in a Pt/Al_2O_3@Cu/ZSM-5 core-shell catalyst: modeling and optimization. Chem Eng J 418:129065
Jin QJ, Shen YS, Mei CQ, Zhang YC, Zeng YW (2020) Catalytic removal of NO and dioxins over W-Zr-Ox/Ti-Ce-Mn-Ox from flue gas: performance and mechanism study. Catal Today 388–389:372–382
Liang WY, Wang GH, Peng C, Tan JQ, Wan J, Sun PF, Li QN, Ji XW, Zhang Q, Wu YH, Zhang W (2022) Recent advances of carbon-based nano zero valent iron for heavy metals remediation in soil and water: a critical review. J Hazard Mater 426:127993
Liu KJ, Yu QB, Wang BL, Qin Q, Wei MQ, Fu Q (2020) Low temperature selective catalytic reduction of nitric oxide with urea over activated carbon supported metal oxide catalysts. Environ Technol 41:808–821
Li WF, Jin SL, Zhang R, Wei YB, Wang JC, Yang S, Wang H, Yang MH, Liu Y, Qiao WM, Ling LC, Jin ML (2020) Insights into the promotion role of phosphorus doping on carbon as a metal-free catalyst for low-temperature selective catalytic reduction of NO with NH_3. Rsc Adv 10:12908–12919
Lu P, Li R, Xing Y, Li Y, Zhu TY, Yue HF, Wu WR (2018) Low temperature selective catalytic reduction of NO_X with NH_3 by activated coke loaded with $Fe_xCo_yCe_zO_m$: the enhanced activity, mechanism and kinetics. Fuel 233:188–199
Massa W (2014) Crystallographic databases. Acta Crystallogr A 44:230–231
Nishi Y, Suzuki T, Kaneko K (1997) Ambient temperature reduction of NO to N_2 in Ru-tailored carbon subnanospace. J Phys Chem B 101:1938–1939
Panda P, Pal K, Chakroborty S (2021) Smart advancements of key challenges in graphene-assembly glucose sensor technologies: a mini review. Mater Lett 303:130508
Qi G, Yang RT (2003) Performance and kinetics study for low-temperature SCR of NO with NH_3 over MnO_x-CeO_2 catalyst. J Catal 217:434–441
Qin YH, Huang L, Zheng JX, Ren Q (2016) Low-temperature selective catalytic reduction of NO with CO over A-Cu-BTC and AO_x/CuO_y/C catalyst. Inrg Chem Commun 72:78–82
Rosas JM, Ruiz-Rosas R, Rodríguez-Mirasol J, Cordero T (2012) Kinetic study of NO reduction on carbon-supported chromium catalysts. Catal Today 187:201–211
Samojeden B, Grzybek T (2016) The influence of the promotion of N-modified activated carbon with iron on NO removal by NH_3-SCR (selective catalytic reduction). Energy 116:1484–1491
Song GJ, Xiao Y, Yang Z, Yang XT, Lyu QG, Zhang XS, Pan QB (2021) Operating characteristics and ultra-low NOx emission of 75 t/h coal slime circulating fluidized bed boiler with post-combustion technology. Fuel 292:120276
Song YJ, Wang T, Cheng L, Li CQ, Wang H, Wang XC (2019) Simultaneous removal of SO_2 and NO by CO reduction over prevulcanized Fe_2O_3/AC catalysts. Can J Chem Eng 97:2015–2020
Teng H, Suuberg EM (1993) Chemisorption of nitric oxide on char. 1. Reversible nitric oxide sorption. J Phys Chem 97:478–483
Wang XB, Zhang L, Wu SG, Zou WX, Yu SH, Shao Y, Dong L (2016) Promotional effect of Ce on iron-based catalysts for selective catalytic reduction of NO with NH_3. Catalysts 6:112
Wang YL, Ge GZ, Zhan L, Li C, Qiao WM, Liang L (2012) MnO_x–CeO_2/activated carbon honeycomb catalyst for selective catalytic reduction of NO with NH_3 at low temperatures. Ind Eng Chem Res 51:11667–11673
Wu Z, Jiang B, Liu Y, Zhao W, Guan B (2007) Experimental study on a low-temperature SCR catalyst based on MnO_x/TiO_2 prepared by sol-gel method. J Hazard Mater 145:488–494
Ye M, Cheng C, Li Y, Lin Y, Wang X, Chen G (2020) Enhancement of the denitrification efficiency over low-rank activated coke by doping with transition metal oxides. Can J Chem Eng 98:1390–1397
Yuan E, Wu G, Dai W, Guan N, Li L (2017) One-pot construction of Fe/ZSM-5 zeolites for the selective catalytic reduction of nitrogen oxides by ammonia. Catal Sci Technol 7:3036–3044
Zhang Y, Zheng Y, Xie W, Lu X (2015) Preparation of Mn–FeO_x/CNTs catalysts by redox co-precipitation and application in low-temperature NO reduction with NH_3. Catal Commun 62:57–61

Zhang D, Yang RT (2017) NH_3-SCR of NO over one-pot Cu-SAPO-34 catalyst: Performance enhancement by doping Fe and MnCe and insight into N_2O formation. Appl Catal A Gen 543:247–256

Zhang K, Xu LT, Niu SL, Lu CM, Wang D, Zhang Q, Li J (2017a) Iron-manganese-magnesium mixed oxides catalysts for selective catalytic reduction of NO_X with NH_3. Korean J Chem Eng 34:1858–1866

Zhang L, Shu H, Lei Z, Jia Y, Wang YS (2020) MnO_X-CuO_X cordierite catalyst for selective catalytic oxidation of the NO at low temperature. Environ Sci Pollut R 27:23695–23706

Zhang NN, Xin Y, Wang X, Shao MF, Li Q, Ma XC, Qi YG, Zheng LR, Zhang ZL (2017b) Iron-niobium composite oxides for selective catalytic reduction of NO with NH_3. Catal Commun 97:111–115

Zhou XG, Huang XY, Xie AJ, Luo SP, Yao C, Li XZ, Zuo SX (2017) V_2O_5-decorated Mn-Fe/attapulgite catalyst with high SO_2 tolerance for SCR of NO_X with NH_3 at low temperature. Chem Eng J 326:1074–1085

Zou XY, Lou SF, Yang C, Liu NW, Wang X, Shi L, Meng X (2020) Catalytic oxidation of NO on N-doped carbon materials at low temperature. Catal Lett 151:487–496